Published in final edited form as:
Mol Pharm. 2009 ; 6(5): 1353–1362. doi:10.1021/mp900021q.

In vivo evaluation of doxorubicin-loaded polymeric micelles targeting folate receptors and early endosomal pH in drug-resistant ovarian cancer

Dongin Kim, **Zhong Gao Gao**, **Eun Seong Lee**, and **You Han Bae***
Department of Pharmaceutics and Pharmaceutical Chemistry, University of Utah, 421 Wakara Way, Suite 318, Salt Lake City, Utah 84108.

Abstract

The second generation of pH-sensitive micelles composed of poly($_L$-histidine-*co*-$_L$-phenlyalanine (16 mol%))(MW: 5K)-*b*-PEG(MW: 2K) and poly($_L$-lactic acid)(MW: 3K)-*b*-PEG(MW: 2K)-folate (80/20 wt/wt%) was previously optimized by physicochemical and *in vitro* tests for both folate receptor and early endosomal pH targeting (pH ~6.0). In this study, the therapeutic efficacy of the doxorubicin (DOX)-loaded micelles (DOX loading content: 20wt %) was evaluated using *in vivo* tests. Multidrug-resistant (MDR) ovarian tumor-xenografted mouse models were employed. The skin-fold dorsal window chamber model was applied for visualization of extravasation and drug retention for the initial one hour after i.v. injection. Non-invasive imaging followed, providing evidence of drug accumulation in the tumor after the first hour. The biodistribution study further supported the long circulation of the drug carrier, tumor-selective accumulation and intracellular drug delivery. Comprehensive tumor growth inhibition experiments examined the collective efficacy of the pH-sensitive micelles. The micelle formulation effectively suppressed the growth of existing MDR tumors in mice for at least 50 days by three *i.v.* injections at a 3-day interval at a dose of 10 mg DOX/kg. The body weight of the animals treated with the test micelle formulation gradually increased over the experimental time period, rather than decreasing. The micelle formulation was superior to its first generation, which targeted pH 6.8 and folate receptor.

Keywords

multidrug-resistance (MDR); pH-sensitive micelle; endosomal pH targeting; folate receptor targeting; ovarian cancer

Introduction

In order for chemotherapy to be effective, chemotherapeutic agents must be active against cancer cells while having minimal toxic effects on healthy cells, tissues and organs.[1–3] Once carriers loaded with anticancer agents are systemically introduced, their uptake by the reticuloendothelial system (RES) must be minimized. This contributes to prolonged circulation of the carriers in the blood.[4, 5] The longer the drug circulates in the blood, the more likely it is to encounter the tumor as a result of the enhanced permeability of leaky tumor blood vessels. The enhanced permeability and retention (EPR) effect[6–8] is regarded as the primary mechanism of preferential accumulation of long-circulating nanoparticulates in solid tumors.

*To whom correspondence should be addressed. Tel: +(801)-585-1518, Fax: +(801)-585-3614, you.bae@utah.edu.

Multidrug resistance (MDR) in tumors is defined by a decreased sensitivity of cells to not only a chemotherapeutic test drug but also a broad spectrum of drugs irrelevant to the test drug in terms of structural homology and/or common targets. The nature of inherited or acquired MDR tumors significantly limits the bioavailability of the delivered anticancer agents to cancer cells.[9–12] One of major MDR mechanisms involves drug efflux operated by P-glycoprotein (Pgp) located on the cell membrane.[8, 13, 14] To overcome this, co-delivery of Pgp inhibitors (or modulators), such as verapamil and its analogs, with anticancer agents has been attempted.[15, 16] However, this approach is seldom used because of the toxicity of Pgp inhibitors against healthy cells (causing, for example, hypotension, ataxia, and immunosuppression)[16] and the reduced systemic clearance of anticancer drug by Pgp inhibitors, leading to adverse effects related to the anticancer drugs[17]. Conversely, even substrate drugs to Pgp, when utilizing active endocytosis routes, often bypass Pgp.[18, 19] There exist other MDR mechanisms that can expel even cytosolic drugs, which include various molecular pumps, drug sequestration and exocytosis.[20–23] Basic drugs in particular, such as doxorubicin, can be trapped in acidic intracellular organelles of endosomes or lysosomes and are then consequently degraded by the acidic environment (pH 4–5) and by various lysosomal enzymes.[11, 20–24] Exocytosis involves the recycling of drug sequestrating endosomes, consequently removing the drug from the cells. Due to multifactorial MDR mechanisms, anticancer agents have little effectiveness against MDR cancer cells.

Polymeric drug carrier systems that use various approaches to address these challenges have been intensively developed.[18, 19, 25–29] Their nanoscale size and hydrophilic surface, often endowed by PEG, allow long circulation in the blood and accumulation in the tumor sites via the EPR effect.[30, 31] Adding a targeting moiety, such as a ligand or an antibody, helps the cellular uptake while avoiding Pgp.[19, 32–35] The endosomolytic property, if one exists, of polymeric carriers can prevent the drug carriers or drugs from sequestration and exocytosis.[19, 29, 36, 37] Various environmentally (e.g., pH-,[19, 29] enzyme-[38, 39] and temperature-[40, 41]) sensitive drug carriers have been utilized for effective cytosolic delivery of the drugs.

Previously, we developed a poly(L-histidine (His))-based pH-sensitive micellelar drug formulation to treat tumors.[19, 42, 43] The pK value of His (~6.5) and its known membrane disruption property make it an optimal drug delivery system for solid tumors for the following reasons.[42] PolyHis has transitions from hydrophobic properties at high pH (> 7.0) to hydrophilic properties at low pH (<7.0) due to the ionization of the imidazole group at lower pH.[42] The polyHis(MW: 5K)-*b*-PEG(MW: 2K) diblock copolymer forms the micelle and encapsulates hydrophobic drugs at high pH (~8.0). The micelle can be destabilized into unimer diblock copolymers at relatively acidic pH (<7.0). The extracellular tumor pH is known to be more acidic than normal tissue pH, which suggests that the drug encapsulated in the micelles can be released at a higher rate at pH 7.0 than at pH 7.4. However, its relative instability at pH 7.4 forced us to use a mixed micelle appraoch.[43] The mixed micelles composed of PLLA(MW: 3K)-*b*- PEG(MW: 2K)-folate and PolyHis(5K)-*b*-PEG(2K) showed improved micelle stability at pH 7.4 due to the enhanced hydrophobicity by the PLLA block in the micelle cores and folate receptor-mediated endocytosis.[43] The mixed micelle systems were destabilized at a pH range of 6.5–7.0, depending on the polymer blending ratio in the mixed micelles. Consequently, the drug-encapsulated micelle system delivered the drug more effectively to acidic tumor sites with minimal loss at physiological blood pH (~7.4). A fraction of loaded drug was released in the extracellular space, and another fraction was released inside the tumor cells after active endocytosis. This mixed micelle system worked properly for wild-type sensitive as well as MDR tumors[19] to a certain extent. However, the fraction of the drug in the extracellular space seemed unavailable for MDR cells due to the activity of Pgp, reducing its efficacy. Blending PLLA-*b*-PEG at higher than 40% caused the loss of the pH sensitivity of the micelles, and the blending approach failed to make micelles sensitive to endosomal pH. To overcome this limit, L-phenylalanine was introduced to the histidine block by co-polymerization of His N-

carboxylanhydride (NCA) and Phe NCA with different feeding ratios.[29] The Phe content in the copolymers significantly dropped the pK values, providing a rough tuning to the target pH. The mixed micelle system composed of poly(His-co-Phe)-*b*-PEG, where poly(His-co-Phe) block contained 16 mol% of Phe, and PLLA-*b*-PEG-folate was then optimized in terms of the composition of the copolymer and blending ratio to achieve optimal physico-chemical properties to target early endosomal pH, resulting in the second generation of pH-sensitive micelles[29]

This study evaluated the in vivo anticancer efficacy of the endosomal pH-sensitive mixed micelles against MDR tumors. Tumor growth inhibition, in vivo noninvasive imaging, and tumor accumulation and retention studies were investigated.

Materials and Methods

Materials

Doxorubicin·HCl (DOX·HCl), triethylamine, potassium tetraborate, and dimethyl sulfoxide (DMSO) were purchased from Sigma Chemical Co. (St. Louis, MO). RPMI 1640 medium, penicillin-streptomycin, fetal bovine serum (FBS), and phosphate buffer solution (PBS) were purchased from Gibco Co. (New York, NY). Cy 5.5 bis-reactive NHS ester was purchased from VWR Scientific Inc. (Denver, CO). Fluorescein DHPE (N-(fluorescein-5-thiocarbamoyl)-1,2-dihexadecanoyl-sn-glycero-3-phosphoethanoamine, triethyl ammonium salt) was purchased from Invitrogen Co. (San Diego, CA). Poly($_L$-histidine (His)-co-$_L$-phenylalanine (Phe: 16 mol%))-*b*-PEG block copolymer was synthesized in house as previously described in our report.[29] Briefly, the synthesis steps include the ring-opening polymerization of the co-monomers of benzyl His N-carboxyanhydride (NCA) and Phe NCA and the subsequent conjugation with PEG. The deprotection of the benzyl group produced the final block copolymer. The syntheses of poly(L-lactide)(PLLA)-*b*-PEG and PLLA-*b*-PEG-folate were described elsewhere.[44]

Preparation of doxorubicin-loaded mixed pH-sensitive micelle (DOX/m-PHSM(20%)-f)

DOX-loaded micelle formulations were prepared as described before.[43] Before loading DOX into the polymeric micelle, DOX·HCl was stirred with 2 molar equivalents of triethylamine in DMSO overnight to remove HCl from DOX·HCl. The polymers and base DOX were dissolved in DMSO and were dialyzed (MWCO 15,000) for 24 hr against HCl-$Na_2B_4O_7$ buffer solution (pH 9.0), and the buffer solution was replaced with fresh solution every 2 hour. The drug-loaded mixed micelles were ready to use after filtration using a 0.45-μm syringe filter. To measure the amount of entrapped DOX, the micelle solution was lyophilized, and the micelle powder was dissolved in DMSO. The UV absorbance of the DMSO solution was measured at 481 nm to determine the amount of DOX. The particle size of the micelle was determined by dynamic light scattering. The test endosomal pH sensitive micelle was prepared from poly(His-*co*-Phe)-*b*-PEG (80 wt%) and PLLA-*b*-PEG-folate (20 wt%), and control pH-insensitive micelles (PHIM-f) were prepared from PLLA-b-PEG (80 wt%) and PLLA-*b*-PEG-folate (20 wt%).

Cells lines and animals

The human ovarian A2780 DOX–resistant tumor (A2780/DOX^R) cell line was kindly provided by Dr. Kopecek's group (University of Utah), and human epidermoid tumor KB cells were purchased from the American Type Culture Collection (ATCC). Both cell lines were maintained in RPMI 1640 medium with 5% penicillin–streptomycin and 10% fetal bovine serum (FBS) in a humidified incubator at 37°C and a 5% CO_2 atmosphere. Four- to six-week-old female nude mice (BALB/c nu/nu mice) were purchased from Charles River Laboratories

(Wilmington, MA). Nude mice were maintained under the guidelines of an approved protocol from the University of Utah Institutional Animal Care and Use Committee.

In vivo tumor growth test

Mice were accommodated in autoclaved micro-isolator cages that were housed in a positive pressure containment rack and maintained under the guidelines of an approved protocol from the University of Utah Institutional Animal Care and Use Committee. They were randomly assigned to experimental and control groups of 5 or 7 animals each. The xenografts of human ovarian A2780/DOX^R MDR carcinoma were developed by subcutaneously implanting 2×10^6 A2780/DOX^R cells in the right rare flanks of the nude mice, as described previously.[45] When the tumor volume reached 50–100 mm^3, the mice were treated 3 times (Days 0, 3, and 6) at a 3-day interval with DOX-dissolved PBS, DOX-encapsulated m-PHSM-f (DOX/m-PHSM(20%)-f) or PHIM-f (DOX/PHIM-f) micelles. All formulations were injected intravenously via the tail vein at a dose of 10 mg/kg through 25G5/8 needles. The tumor inhibition activity was assessed with the tumor volume, which was calculated by the following equation: $V = (w)^2 \times (l)/2$, where (w) and (l) are the width and length of the tumor as measured by a caliper. The body weight was measured simultaneously.

Skin fold window chamber study

To investigate the in situ delivery of polymeric micelles to solid tumors, a non-invasive visualization method using a 'dorsal skin-fold window chamber model' was employed.[46] To establish the window chamber model,[47] a flap of skin measuring 1 cm in diameter was dissected away from opposing surfaces of the dorsal skin flap of an anesthetized mouse, leaving a facial plane with its associated vasculature. The flaps were held vertically away from the body with a titanium saddle, which was sutured to both sides of the flap. A2780/DOX^R tumor cells or small tumor pieces (~1 mm^3) that were extracted from xenografted mice bearing the A2780/DOX^R tumor were implanted into the window chamber. Glass windows were then attached to the center of the saddle to cover the surgical site. After surgery, the skin surfaces that were adjacent to the window assembly were covered with neomycin sulfate ointment to prevent infection.[46] DOX was incorporated into the polymeric micellar core, and DOX fluorescent imaging was captured in the skin dorsal window. For serial observation of the window, nude mice that were intravenously administered with DOX-loaded micelles (pH-sensitive micelles and pH-insensitive micelles) (60 mg micelles per kg body) were anesthetized with a mixture of 90 mg/kg ketamine (Abbott, IL) and 10 mg/kg xylazine (Bayer, KS). Nude mice were placed on a glass stage with an adjustable restrainer and kept warm using a temperature-controlled heating blanket (homeothermic system, Harvard Apparatus) at 37°C on the microscope stage. Nude mice were positioned so that the mammary window was aligned with the hole of the restraining bar. Observation was made using intravital fluorescence microscopy (Olympus BX51WI Microscope, Leeds Precision Instruments, Inc. MN) over time.

Non-invasive imaging

Cy5.5 (a fluorescent probe for in vivo imaging) bis-NHS ester (2 mol) was reacted with primary amines of poly(benzyl-His)(MW 5K) (1 mol) in a water/DMSO (1 ml/5 ml) mixture solution for 8 hr. After the reaction, unconjugated Cy5.5 bis-NHS ester was removed by dialysis (molecular cut-off: 8000) for 2 days. Cy5.5 labeled poly(benyzl-His) was lyophilized by freeze-drying. The conjugation of Cy5.5 to the polymer was determined by measuring the extinction coefficient at 675 nm, according to the manufacturer's instructions (Amersham Biosciences Co., Piscataway, NJ). Preparation of Cy5.5 labeled m-PHSM-f was performed with Cy5.5 labeled poly(benzyl-His), PLLA-*b*-PEG-folate, poly(His-co-Phe)-*b*-PEG (10/20/70 wt/wt/wt %), and DOX. NaCl (0.9 M) was conducted as previously described. Using a similar ratio between polymers, PHIM-f was prepared with Cy 5.5 labeled poly(benzyl-His), PLLA-*b*-PEG-

folate, PLLA-*b*-PEG (10/20/70 wt/wt/wt%), and DOX. For *in vivo* animal experiments, KB tumor cells were inoculated into female nude mice by subcutaneous injection of 1×10^6 cells suspended in cell culture media (RPMI-1640, 10% fetal bovine serum). When the tumor volume in the two injection sites reached 50–70 mm^3, 10 mg/kg of an equivalent DOX concentration of Cy5.5-labeled micelles was intravenously injected into KB tumor-bearing nude mice through a tail vein. After intravenous administration of Cy5.5 labeled micellar solutions, the time-dependent tissue distribution in tumor-bearing nude mice was imaged by positioning the mice on an animal plate that was heated to 37°C using the Explore Optix System (ART Advanced Research Technologies Inc., Montreal, Canada). Nude mice were moved to the imaging chamber for scanning. Laser power and count time settings were optimized at 25 mW and 0.3 sec per point. Excitation and emission spots were raster-scanned in 1 mm steps over the selected region of interest to generate emission wavelength scans. A 670 nm pulsed laser diode was used to excite Cy5.5 molecules. Near infrared (NIR) fluorescence emission at 700 nm was detected with a fast photo multiplier tube (Hamamatsu, Japan) and a time-correlated single photon counting system (Becker and HicklGmbH, Berlin, Germany).[48]

Biodistribution and drug disposition into organs

The first experiment was accomplished by using a hydrophobic DHPE dye encapsulated mixed micelle system (DHPE/Micelle = 1/10 wt/wt% and micelle concentration = 20 μg/ml). This formulation was injected intravenously via the tail vein (60 mg of micelles per kg of body) of mice bearing large tumors (> 4000 mm^3). At 4 hr post-treatment, the tissues of each organ and the tumor were collected and homogenized into monolayer cell samples. The confocal measurement of each sample was taken. The second experiment included DOX disposition into each organ, including the tumor, and the concentration of drug in the blood. Ovarian A2780/DOX^R MDR tumor xenografts were established in athymic BALB/c nu/nu mice. When the tumors grew larger than 4000 mm^3, DOX/m-PHSM(20%)-f, DOX/PHIM-f, or free DOX dissolved in PBS was injected into the the tail vein at an equivalent dose of 10 mg DOX per kg of body. Mice were anesthetized at a given time point (1 hr, 4 hr, and 24 hr) after treatment. Tissue samples were harvested and suspended in 70% ethanol with 0.3 N HCl and then homogenized to extract doxorubicin. Following centrifugation, doxorubicin fluorescence (excitation at 470 nm, emission at 590 nm) in the supernatant was measured with a fluorescence plate reader (SpectraMax M2, Molecular Devices, Sunnyvale, CA, USA).[49] Blood was collected via cardiac puncture, kept in microtainer tubes with EDTA, and centrifuged to obtain plasma. After freeze-drying the plasma sample, it was dissolved into 70% ethanol with 0.3 N HCl to extract doxorubicin. The doxorubicin fluorescence in the supernatant was measured as mentioned above. At both measurements, doxorubicin concentrations were derived by a pre-measured doxorubicin standard curve. In order to remove the original organ cell fluorescence at the same wavelength, each organ and blood fluorescence were measured without treatment with DOX, and the results were used to normalize the drug disposition results.

Results

Micelle responsive to early endosomal pH

The average size of a DOX-loaded endosomal pH-sensitive mixed micelle was ~150 nm which is in a typical size range of secondary micelles formed by dialysis method. DOX loading content was approximately 20 wt%, and the loading efficiency was ~ 80 wt%. As a control, a pH-insensitive micelle system composed of PLLA-b-PEG/PLLA-b-PEG-folate (80/20 wt/wt%) was used. A previous study optimized the endosomal pH-sensitive micelle in terms of polymer composition and blending ratio judged from pH-dependent physicochemical properties, folate receptor mediated endocytosis, endosomal membrane disruption and cytotoxicity.[29]

In vivo tumor growth inhibition

To test in vivo tumor growth inhibition, DOX-resistant ovarian carcinoma cells (A2780/DOX^R) were xenografted in nude mice. The animals were divided into three groups and treated with free DOX, DOX-loaded pH-sensitive micelles (a test micelle formulation), and pH-insensitive micelles (a control micelle formulation), respectively, by intravenous injections three times. The first treatment was conducted on Day 0, and following treatments were on Day 3 and Day 6. All animals received the same dose of DOX (10 mg/kg). Figure 1 (a) shows the tumor growth rates of all groups. While the animals were treated for 6 days, the average sizes of tumors of all groups are not noticeably distinguishable from each other. However, the growth rate of the test group was significantly reduced after this induction period. The growth apparently stopped until Day 20, followed by slow growth up to Day 30. On Day 49, the tumor size reached about 300 mm^3. The group treated with free DOX showed an exponential curve in growth, and all animals in this group were sacrificed on Day 27 due to discomfort tumor burden to animals. The growth rate of the control micelle group was delayed when compared with free DOX group, but the growth was accelerated after treatments, and the average tumor size on Day 49 was about 9 times bigger than in the test group.

Figure 1 (b) presents the changes in the body weight of each group over time as an indication of overall systemic toxicity of the formulations. The free DOX group demonstrated a sharp decrease in the body weight for the initial time period of 9 days and recovery after this period. This strongly suggests serious toxicity of free DOX at the given dose, with losses of more than 20% of the mice's body weight while the tumor was growing. For the control micelle group, the weight loss was minimal during treatments followed by rapid gain, which seems due to the growth of the tumor for the next two weeks. When tumors grew further, the weight gain slowed, probably owing to ill conditions. On the other hand, the test group showed a slow but steady gain of body weight with minimal growth of tumors for 7 weeks.

Skin fold window chamber study

To directly explore the extent of drug extravasation from the blood vessels and accumulation of DOX in the tumor, the time-dependent fluorescence intensity of DOX in the tumor sight was measured by using a non-invasive skin fold window chamber model, which allows real-time measurements. In Figure 2, the DOX fluorescence images from each formulation were taken at given time intervals (0, 7, 10, 20, and 60 min). The intensity started to appear at 10 min for both DOX-loaded pH-sensitive micelles and pH-insensitive micelles, indicating that extravasation from the blood vessels to the tumor cells occurred, while the fluorescence intensity from the free DOX started to appear at 7 min or before. An important observation in this study was the accumulation of DOX in the tumor. The fluorescence intensity of the pH-sensitive micelle group was maintained up to 60 min. However, the pH-insensitive micelle group started to show decreased fluorescence intensity at 60 min. The intensity from free DOX formulation declined after 20 min and became dark at 60 min, indicating the clearance of free drug from the tumor.

Noninvasive imaging test

To estimate in vivo tumor accumulation beyond the time frame of the window chamber model, a non-invasive and real time imaging method was applied. It assisted us in visualizing biodistribution of drug carriers after one hour post-injection. Using near-infrared (NIR) fluorophore (Cy5.5)-labeled drug carriers, the NIR fluorescence imaging system showed the fate of drug carriers. The in vivo model was tumor cell xenografted nude mice. Figure 3 is the NIR fluorescence images obtained by Cy5.5-labeled pH-sensitive micelles. Compare to the result from Cy5.5-labeled pH-insensitive micelles as a control group previously published in elsewhere,[50] at one hour after injection, pH-sensitive micelles gave higher fluorescence intensity in tumors than the intensities from the whole body. This distinct fluorescence intensity

of tumors was maintained up to 12 hr. No significant fluorescence intensity difference between the tumor and other tissues was observed during the entire time frame. The window model illustrated that the significant drug fluorescence intensity was maintained for the initial one hour from pH-sensitive micelles, which coincides with the tumor accumulation result from Figure 3. In the case of pH-insensitive micelles, the decreased drug fluorescence intensity after one hour from the window chamber model study corresponds to the weak intensities in previous results. [50]

Biodistribution and drug disposition into organs

To monitor the biodistribution of the formulations in the mice, we carried out 2 independent studies. One was to take confocal images of cellular samples of each organ and the tumor after i.v. injection of DHPE fluorescence dye encapsulated pH-sensitive micelles into tumor bearing nude mice. At 4 hr post-injection, the animal was sacrificed, and each organ tissue and tumor tissue were collected. The homogenization of the tissues provided cellular samples to obtain confocal images. Figure 4 distinctively illustrates the difference between DHPE fluorescence intensity from each organ and the tumor. The significantly increased intensity of tumor indirectly indicated the tumor targeting capability of the pH-sensitive micelle.

In another set of experiments, the animals were treated with each drug formulation (DOX encapsulated pH-sensitive micelles, pH-insensitive micelles, or free drug), and the organs and blood were collected at certain time intervals (4, 8, and 12 hours). The DOX fluorescence intensity of each sample was measured by fluorometry.[48] In Figure 5 (a), the drug distribution into the tumor using the pH-sensitive micelle formulation exhibited a higher amount than other organs in all time frames. Figure 5 indicates that the tumor drug distribution amount of the pH-sensitive micelle formulation represented 4-fold and 10-fold increases over the pH-insensitive micelles and free DOX, respectively, even up to 24 hr after treatment. In the case of the pH-insensitive micelle formulation and free DOX shown in Figure 5 (b) and (c), respectively, the liver is the organ that had the highest drug amount among all organs. Interesting results from Figure 5 also point out that both micelle formulations reduced significant amounts of drug distribution into the heart compared with free DOX. In addition, free DOX represented a 3- to 4-fold lower drug concentration in the blood at 1 hr and 4 hr time points than both micelle formulations.

Discussion

Simultaneously targeting tumor extracellular pH and the folate receptor using pH-sensitive micelles composed of polyHis-*b*-PEG and PLLA-*b*-PEG-folate was effective in treating drug-sensitive and MDR counterparts of MCF-7 breast[19] and A2780 ovarian[29] tumors in mice. The proposed mechanisms for treating MDR tumors include active endocytosis, accelerated drug release, and endosomolytic function of polyHis. The combined mechanisms maximize the cytosolic delivery of incorporated drugs. The pH of physical destabilization of the micelles was manipulated by the blending ratio of two block copolymers,[29, 43] which are miscible by demonstrating a single glass transition temperature (Tg) located between the two separate Tgs of polyHis and PLLA.[51] However, shifting the destabilizing pH below 6.6 by the blending approach while preserving pH sensitivity at a target pH was not feasible. As the content of PLLA in the micelle core increased, the sensitivity declined and was eventually lost above 40 wt% of PLLA. It was hypothesized that any drug fraction released in the extracellular space from carriers is not bioavailable for MDR cancer cells, which are equipped with Pgp on the plasma surface. To maximize the bioavailability of the drug to the cytosolic compartment, the pH-induced destabilization should occur after active endocytosis, while maintaining minimal release in the tumor extracellular space (pH 6.5–7.2). It was found that the incorporation of a hydrophobic amino acid monomer, such as Phe in this study, effectively shifted the pK of

polyHis to a lower pH region. To precisely target early endosomal pH (pH 6.0), the combined approaches of copolymerization and blending were employed. A copolymer composition was selected while keeping a PLLA-*b*-PEG-f content at 20 wt%, which provided folate on the surface of the micelle for the second generation of PHSM-f fabrication. The resulting micelle surface had an optimal folate surface density for folate receptor-mediated endocytosis.[50]

The PHSM-f targeting pH 6.0 effectively suppressed the growth rate of MDR ovarian tumors for a long term by three injections in the initial 6 days. The average tumor size reached only 250–300 mm^3 after 50 days. When the tumors were treated with the first generation of PHSM-f, which targets pH 6.8, the tumor grew after 50 days to 1,300 mm^3 (data not shown). This clearly suggests that the second generation of the micelles is more effective in treating MDR cancer cells.

The MDR mechanisms, especially in clinical settings, are multifaceted: they include unicellular mechanisms and extracellular mechanisms associated with the interactions with extracellular matrices, other cells, and soluble factors. A Pgp pump is one of numerous unicellular mechanisms. The use of Pgp inhibitors has yet to be approved in clinical application even after significant research and investment for the last decades. Costly systemic high dose therapy while saving patients' bone marrow has also been challenged to better treat resistant tumors. [17] However, at present, the approach has been concluded to be ineffective.[52] The alternative approach that we have taken is the cytosolic high dose therapy in order to address such limitations as the high systemic toxicity of high dose therapy and to challenge multifactorial MDR mechanisms. The hypothesis is that although MDR cancer cells develop various defense mechanisms against cytotoxic agents, the defense by an individual mechanism or combined mechanisms might have limited capacity if the cells have not previously experienced high cytosolic concentrations, which cannot be encountered under ordinary environmental conditions. Thus, a high cytosolic drug concentration that exceeds the limited defense capacity is expected to treat MDR cancer cells.

To support the hypothesis at least in part, the rest of the experimental design was centered on demonstrating the accumulation of doxorubicin in the tumor site and the cytosol. The initial deposition for one hour of DOX immediately after IV injection was visualized by using the dorsal window chamber model. Because the observation was made under a microscope while maintaining an anesthetic condition of mice, its observation time is limited but provides the dynamics of accumulation. It is interesting to note that the fluorescence intensity of DOX carried by PHIM-f at the tumor site reached the maximum between 7 and 20 min post-injection, while the highest DOX intensity carried by PHSM-f was obtained at or after 60 min, even though both systems had folate conjugated on their surfaces. The reasons for this observation are not clearly understood. Because two micelle systems share a common endocytosis pathway, the different kinetics at the tumor sites seem to be attributable to the intracellular events of accelerated drug release rates and endosomolysis. Such events may minimize drug efflux and endosomal recycling, increase diffusion spreading of the drug, and provide room for particles arriving later. Cy5.5 imaging results (Figure 3) coincide well with the observation from the window model, showing that the highest accumulation of DOX carried by PHSM-f at the tumor site occurred around one hour post-injection, while the drug concentration in the tumor delivered by PHIM-f was already in the declining phase at one hour, [50] although a different tumor was used in this imaging study.

Figure 4 shows the green fluorescence of cells harvested from each organ 4 hours post-injection and clearly demonstrates that a significant fraction of DHPE dye carried by PHSM-f resides inside cells. The result supports the highest uptake of the micelles by cancer cells compared to cells in other organs. More quantitative analysis of DOX accumulation in each organ is presented in Figure 5. The DOX accumulation in the tumor was higher than in all other organs

when PHSM-f was used, as shown in Figure 4; however, the liver uptake became dominant for PHIM-f and free DOX. Despite similar blood concentration profiles over time (Figure 5 (d)) between two micelle formulations, the large difference (~3/1 for PHSM-f and ~1/3 for PHIM-f) in tumor/liver ratios of drug accumulation is an interesting feature but a subject for further investigation.

In summary, PHSM-f, which simultaneously targets the folate receptor and early endosomal pH, has proven its efficacy in treating ovarian multidrug resistant tumor without weight loss. The growth rate of already formed MDR ovarian solid tumor was well suppressed for whole experimental time period (49 days) after three injections (10 mg DOX/kg each injection) on Days 0, 3, and 6. The system was more effective than the first generation micelles targeting extracellular pH and the folate receptor. The biodistribution results provided from the dorsal window chamber model, non-invasive imaging, and organ extraction method were consistent and strongly supported high accumulation of DOX at tumor sites and cytosolic delivery.

Acknowledgments

This work was supported by NIH CA 101850. Drs. K. Park and I.C. Kwon in KIST (Korea) are acknowledged for their help with non-invasive imaging experiments.

References

1. Peer D, Karp JM, Hong S, Farokhzad OC, Margalit R, Langer R. Nanocarriers as an emerging platform for cancer therapy. Nat. Nanotech 2007;2:751–760.
2. Allen TM, Cullis PR. Drug delivery systems: Entering the mainstream. Science 2004;303:1818–1822. [PubMed: 15031496]
3. Ferrari M. Cancer nanotechnology: opportunities and challenges. Nat. Rev. Cancer 2005;5:161–175. [PubMed: 15738981]
4. Moghimi SM, Hunter AC, Murray JC. Long-circulating and target-specific nanoparticles: Theory to practice. Pharmacol. Rev 2001;53:283–318. [PubMed: 11356986]
5. Gabizon AA. Selective tumor localization and improved therapeutic index of anthracyclines encapsulated in long circulating liposomes. Cancer Res 1992;52:891–896. [PubMed: 1737351]
6. Maeda H, Wu J, Sawa T, Matsumura Y, Hori K. Tumor vascular permeability and the EPR effect in macromolecular therapeutics: a review. J. Control. Release 2000;65:271–284. [PubMed: 10699287]
7. Dvorak HF, Nagy JA, Dvorak JT, Dvorak AM. Identification and characterization of the blood vessels of solid tumors that are leaky to circulating macromolecules. Am. J. Pathol 1988;133:95–109. [PubMed: 2459969]
8. Heuser LS, Miller FN. differential macromolecular leakage from the vasculature of tumors. Cancer 1986;57:461–464. [PubMed: 2417677]
9. Gottesman MM, Pastan I, Ambudkar SV. P-glycoprotein and multi drug resistance. Curr. Opin. Genet. Dev 1996;6:610–617. [PubMed: 8939727]
10. Narasaki F, Matsuo I, Ikuno N, Fukuka M, Soda H, Oka M. Multidrug resistance-associated protein (MRP) gene expression in human lung cancer. Anticancer Res 1996;16:2079–2082. [PubMed: 8712746]
11. Ouar Z, Lacave R, Bens M, Vandewalle A. Mechanisms of altered sequestration and efflux of chemotherapeutic drugs by multidrug-resistant cells. Cell Biol. Toxicol 1999;15:91–100. [PubMed: 10408356]
12. Hager A, Debus G, Edel HG, Stransky H, Serrano R. Auxin induces exocytosis and the rapid synthesis of a high-turnover pool of plasma-membrane H^+ ATPase. Planta 1991;185:527–537.
13. Tanigawara Y. Role of p-glycoprotein in drug disposition. Ther. Drug Monit 2000;22:137–140. [PubMed: 10688277]
14. Schwarzenbach H. Expression of MDR1/P-glycoprotein, the multidrug resistance protein MRP, and the lung-resistance protein LRP in multiple myeloma. Med. Oncol 2002;19:87–104. [PubMed: 12180485]

15. Sikic BI, Fisher GA, Lum BL, Halsey J, Beketic-Oreskovic L, Chen G. Modulation and prevention of multidrug resistance by inhibitors of P-glycoprotein. Cancer Chemother. Pharmacol 1997;40:S13–S19. [PubMed: 9272128]
16. Krishna R, Mayer LD. Multidrug resistance (MDR) in cancer Mechanisms, reversal using modulators of MDR and the role of MDR modulators in influencing the pharmacokinetics of anticancer drugs. Eur. J. Pharm. Sci 2000;11:265–283. [PubMed: 11033070]
17. Robert J, Jarry C. Multidrug resistance reversal agents. J. Med. Chem 2003;46:4805–4817. [PubMed: 14584929]
18. Mamot C, Drummond DC, Hong K, Kirpotin DB, Park JW. Liposome-based approaches to overcome anticancer drug resistance. Drug Resist. Update 2003;6:271–279.
19. Lee ES, Na K, Bae YH. Doxorubicin loaded pH-sensitive polymeric micelles for reversal of resistant MCF-7 tumor. J. Control. Release 2005;103:405–418. [PubMed: 15763623]
20. Mohajer G, Lee ES, Bae YH. Enhanced intercellular retention activity of novel pH-sensitive olymeric micelles in wild and multidrug resistance MCF-7 cells. Pharm. Res 2007;4:1618–1627. [PubMed: 17385015]
21. Simon SM, Schindler M. Cell biological mechanisms of multidrug resistance in tumors. Proc. Natl. Acad. Sci. USA 1994;91:3497–3504. [PubMed: 7909602]
22. Beck WT. The cell biology of multiple drug resistance. Biochem. Pharmacol 1987;36:2879–2887. [PubMed: 2888464]
23. Simon SM, Roy D, Schindler M. Intracellular pH and the control of multidrug resistance. Proc. Natl. Acad. Sci. USA 1994;91:1128–1132. [PubMed: 8302842]
24. Breuninger LM, Paul S, Gaughan K, Miki T, Chan A, Aaronson SA, Kruh GD. Expression of multidrug resistance-associated protein in NIH/3T3 cells confers multidrug resistance associated with increased drug efflux and altered intracellular drug distribution. Cancer Res 1995;55:5342–5347. [PubMed: 7585598]
25. Minko T, Batrakova EV, Li S, Li Y, Pakunlu RI, Alakhov VYu, Kabanov AV. Pluronic block copolymers alter apoptotic signal transduction of doxorubicin in drug-resistant cancer cells. J. Control. Release 2005;105:269–278. [PubMed: 15939500]
26. Chavanpatil MD, Patil Y, Panyam J. Susceptibility of nanoparticle-encapsulated paclitaxel to P-glycoprotein-mediated drug efflux. Int. J. Pharm 2006;320:150–156. [PubMed: 16713148]
27. Wong HL, Bendayan R, Rauth AM, Xue HY, Babakhanian K, Wu XY. A mechanistic study of enhanced doxorubicin uptake and retention in multidrug resistant breast cancer cells using a polymer-lipid hybrid nanoparticle system. J. Pharmacol. Exp. Ther 2006;317:1372–1381. [PubMed: 16547167]
28. Stastny M, Plocova D, Etrych T, Ulbrich K, Rihova B. HPMA-hydrogels result in prolonged delivery of anticancer drugs and are a promising tool for the treatment of sensitive and multidrug resistant leukaemia. Eur. J. Cancer 2002;38:602–608. [PubMed: 11872356]
29. Kim D, Lee ES, Oh KT, Gao ZG, Bae YH. Doxorubicin-loaded polymeric micelle overcomes multidrug resistance of cancer by double-targeting folate receptor and early endosomal pH. Small 2008;4:2043–2050. [PubMed: 18949788]
30. Otsuka H, Nagasaki Y, Kataoka K. PEGylated nanoparticles for biological and pharmaceutical applications. Adv. Drug Delivery Rev 2003;55:403–419.
31. Brannon-Peppas L, Blanchette JO. Nanoparticle and targeted systems for cancer therapy. Adv. Drug Delivery Rev 2004;56:1649–1659.
32. Goren D, Horowitz AT, Tzemach D, Tarshish M, Zalipsky S, Gabizon A. Nuclear delivery of doxorubicin via folate-targeted liposomes with bypass of multidrug-resistance efflux pump. Clin. Cancer Res 2000;6:1949–1957. [PubMed: 10815920]
33. Guillemard V, Saragovi HU. Prodrug chemotherapeutics bypass p-glycoprotein resistance and kill tumors in vivo with high efficacy and target-dependent selectivity. Oncogene 2004;23:3613–3621. [PubMed: 15034547]
34. Sapra P, Allen TM. Ligand-targeted liposomal anticancer drugs. Prog. Lipid Res 2003;42:439–462. [PubMed: 12814645]
35. Peer D, Karp JM, Hong S, Farokhzad OC, Margalit R, Langer R. Nanocarriers as an emerging platform for cancer therapy. Nat. Nanotechnol 2007;2:751–760. [PubMed: 18654426]

36. Murthy N, Robichaud JR, Tirrell DA, Stayton PS, Hoffman AS. The design and synthesis of polymers for eukaryotic membrane disruption. J. Control. Release 1999;61:137–143. [PubMed: 10469910]
37. Carneiro FA, Stauffer F, Lima CS, Juliano MA, Juliano L, Da Poian AT. Membrane fusion induced by vesicular stomatitis virus depends on histidine protonation. J. Biol. Chem 2003;278:13789–13794. [PubMed: 12571240]
38. Gopin A, Ebner S, Attali B, Shabat D. Enzymatic activation of second-generation dendritic prodrugs: Conjugation of self-immolative dendrimers with poly(ethylene glycol) via click chemistry. Bioconjugate Chem 2006;17:1432–1440.
39. de Groot FM, Damen EW, Scheeren HW. Anticancer prodrugs for application in monotherapy: targeting hypoxia, tumor-associated enzymes, and receptors. Curr. Med. Chem 2001;8:1093–1122. [PubMed: 11472243]
40. Chilkoti A, Dreher MD, Meyer DE, Raucher D. Targeted drug delivery by thermally responsive polymers. Adv. Drug Deliver. Rev 2002;54:613–630.
41. Na K, Lee KH, Lee DH, Bae YH. Biodegradable thermo-sensitive nanoparticles from poly(l-lactic acid)/poly(ethylene glycol) alternating multi-block copolymer for potential anticancer drug carrier. Eur. J. Pharm. Sci 2006;27:115–122. [PubMed: 16253487]
42. Lee ES, Shin HJ, Na K, Bae YH. Poly(L-histidine)-PEG block copolymer micelles and pH-induced destabilization. J. Control. Release 2003;90:363–374. [PubMed: 12880703]
43. Lee ES, Na K, Bae YH. Polymeric micelle for tumor pH and folate-mediated targeting. J. Control. Release 2003;91:103–113. [PubMed: 12932642]
44. Han SK, Na K, Bae YH. Sulfonamide based pH-sensitive polymeric micelles: physicochemical characterizations and pH-dependent aggregation. Colloids Surf., A 2003;214:49–59.
45. Gao ZG, Fain HD, Rapoport N. Controlled and targeted tumor chemotherapy by micellar-encapsulated drug and ultrasound. J. Control. Release 2005;102:203–222. [PubMed: 15653146]
46. Dreher MR, Liu W, Michelich CR, Dewhirst MW, Yuan F, Chilkoti A. Tumor vascular permeability, accumulation, and penetration of macromolecular drug carriers. J. Natl. Cancer Inst 2006;98:335–344. [PubMed: 16507830]
47. Shan S, Sorg B, Dewhirst MW. A novel rodent mammary window of orthotopic breast cancer for intravital microscopy. Microvasc. Res 2003;65:109–117. [PubMed: 12686168]
48. Park K, Kim JH, Nam YS, Lee S, Nam HY, Kim K, Park JH, Kim IS, Choi K, Kim SY, Kwon IC. Effect of polymer molecular weight on the tumor targeting characteristics of self-assembled glycol chitosan nanoparticles. J. Control. Release 2007;122:305–314. [PubMed: 17643545]
49. Cheong I, Huang X, Bettegowda C, Diaz LA Jr, Kinzler KW, Zhou S, Vogelstein B. A bacterial protein enhances the release and efficacy of liposomal cancer drugs. Science 2006;314:1308–1311. [PubMed: 17124324]
50. Kim D, Lee ES, Park K, Kwon IC, Bae YH. Doxorubicin Loaded pH-sensitive Micelle: Antitumoral Efficacy against Ovarian A2780/DOX^{R} Tumor. Pharm. Res 2008;25:2074–2082. [PubMed: 18449626]
51. Yin H, Lee ES, Kim D, Lee KH, Oh KT, Bae YH. Physicochemical characteristics of pH-sensitive poly(L-Histidine)-b-poly (ethylene glycol)/poly(L-Lactide)-b-poly(ethylene glycol) mixed micelles. J. Control. Release 2008;126:130–138. [PubMed: 18187224]
52. Szakacs G, Paterson JK, Ludwig JA, Booth-Genthe C, Gottesman MM. Targeting multidrug resistance in cancer. Nat. Rev. Drug Discov 2006;5:219–234. [PubMed: 16518375]

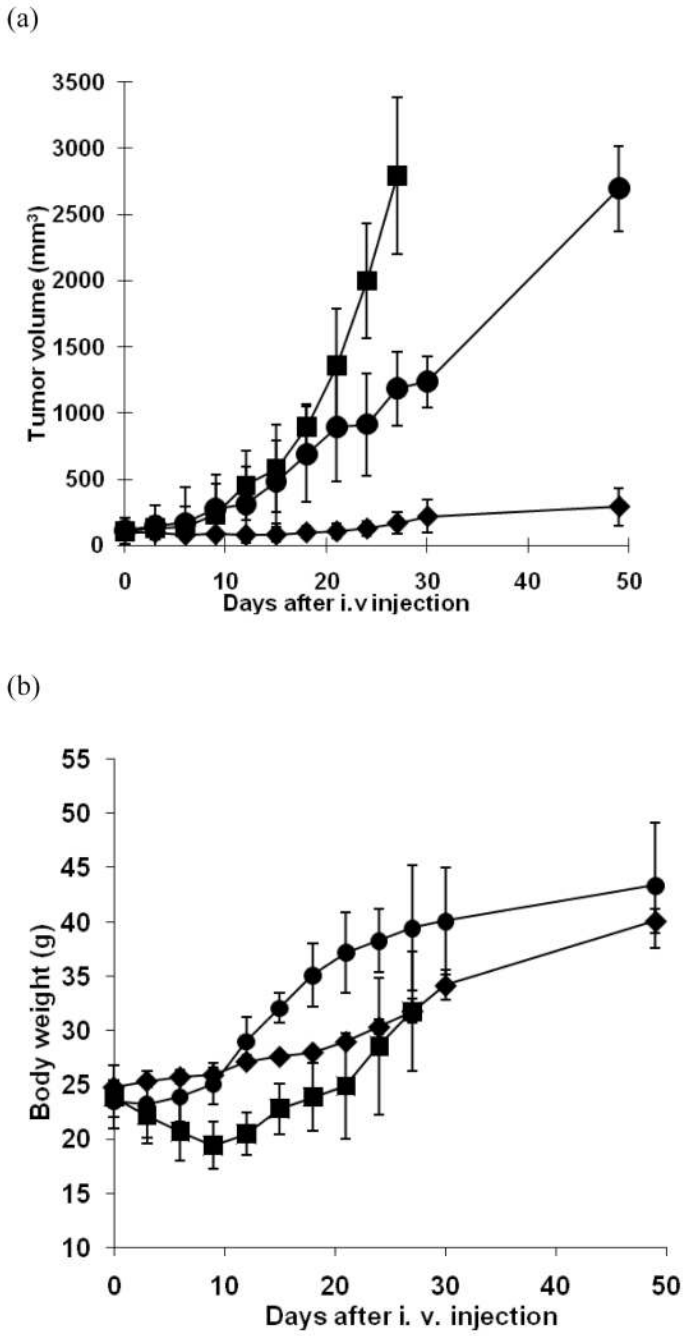

Figure 1.

In vivo tumor growth inhibition test and body weight change of s.c. ovarian A2780/DOX^R xenografted BALB/c nude mice (n = 7). 10 mg/kg of DOX equivalent dose was injected as several formulations including free DOX in PBS (■), DOX-loaded pH-insensitive micelles (DOX/PHIM-f) (●), and DOX-loaded pH-sensitive micelles (DOX/m-PHSM(20%)-f) (♦). Three IV injections on days 0, 3, and 6 were made. Values are the mean ± standard deviation (S.D.). (a) Tumor volume change; (b) body weight changes.

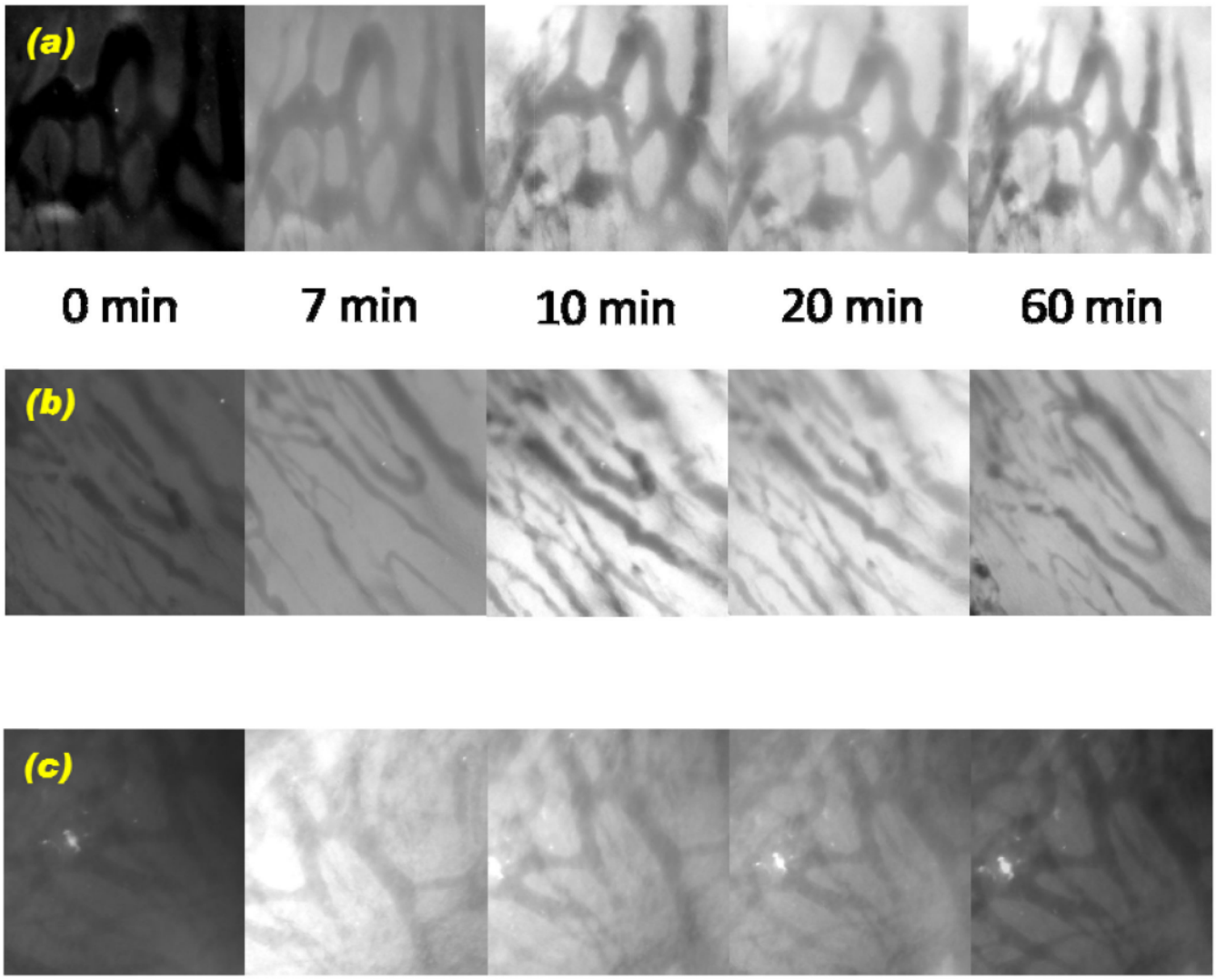

Figure 2.
In vivo skin fold window chamber model study: (a) DOX extravasation from A2780/DOX^R ovarian tumor blood vessel into the tumor using DOX-loaded pH-sensitive micelles (DOX/m-PHSM(20%)-f), (b) DOX-loaded pH-insensitive micelles (DOX/PHIM-f), and (c) free DOX in PBS according to time frames (0, 7, 10, 20, and 60 min).

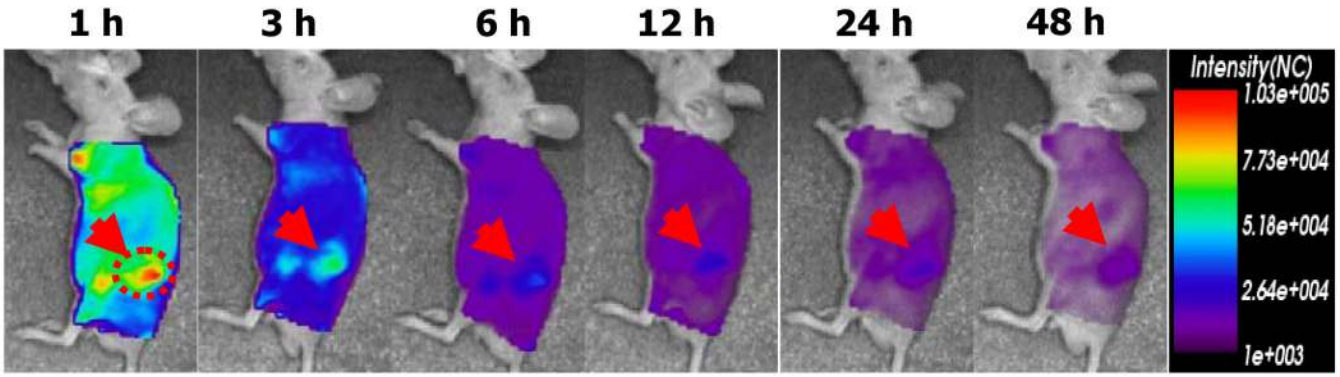

Figure 3.
In vivo optical fluorescence imaging of KB tumor xenografted BALB/c nude mice after DOX encapsulated and Cy 5.5 fluorescent dye labeled pH-sensitive micelles. Arrows indicate the location of the tumor.

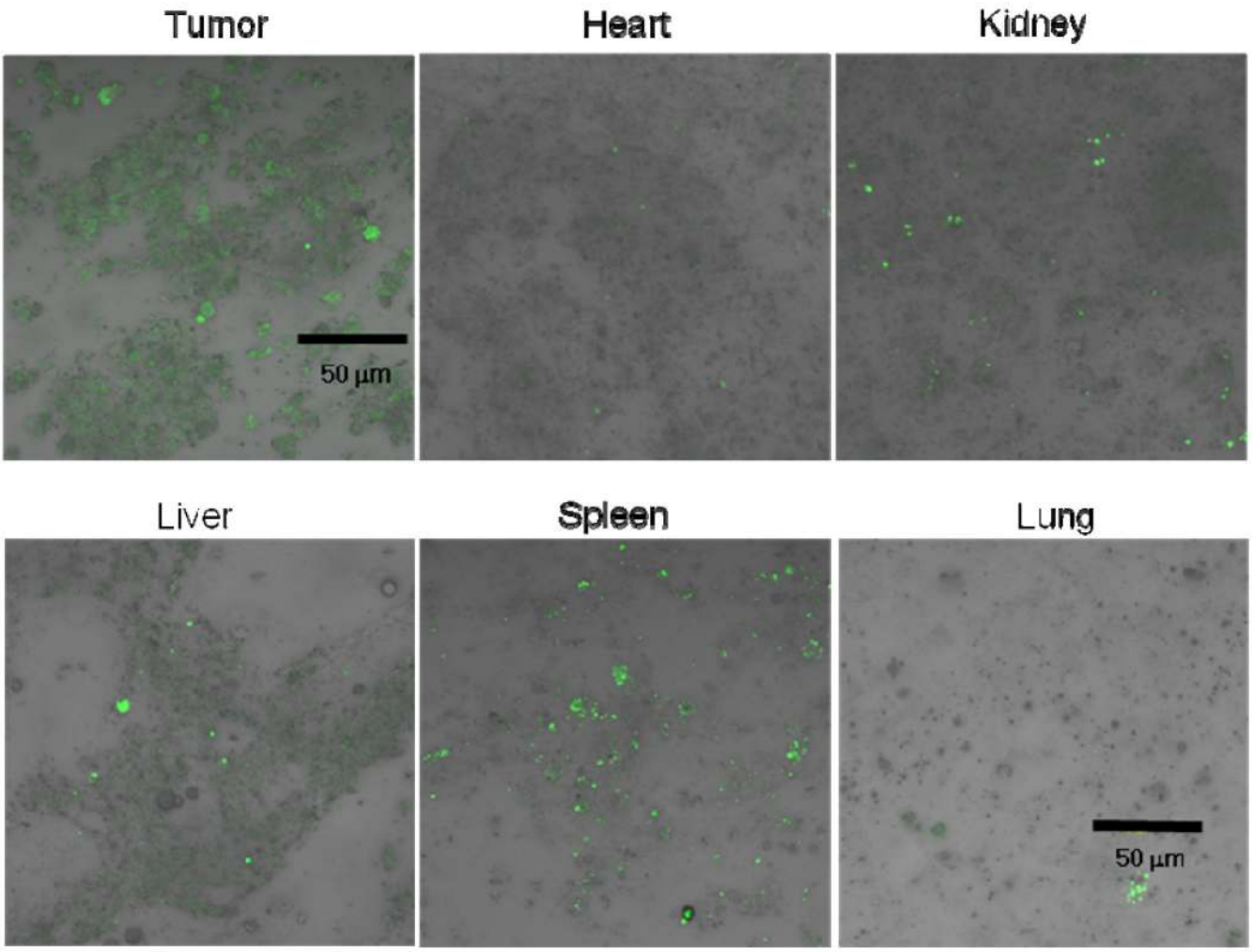

Figure 4.
Biodistribution of DHPE dye encapsulated pH-sensitive micelles injected through the tail vein of ovarian A2780/DOX^R tumor xenografted nude mice. The confocal images of each organ, including the tumor, were prepared as monolayer cellular samples from tissues after sacrifice of animals 4 hr post-treatment.

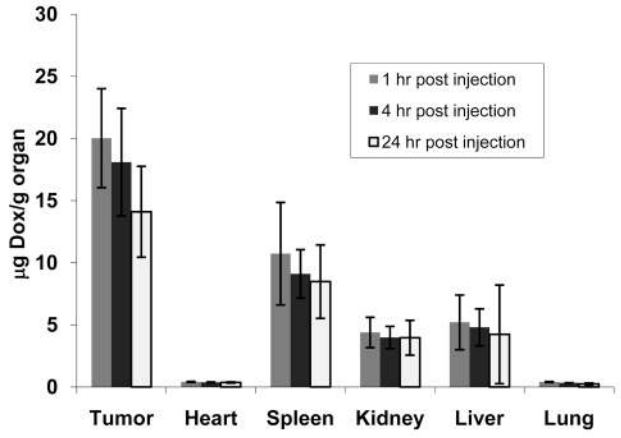

(b)

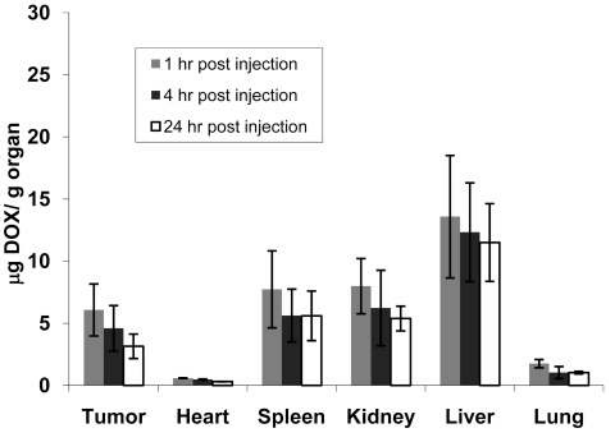

(c)

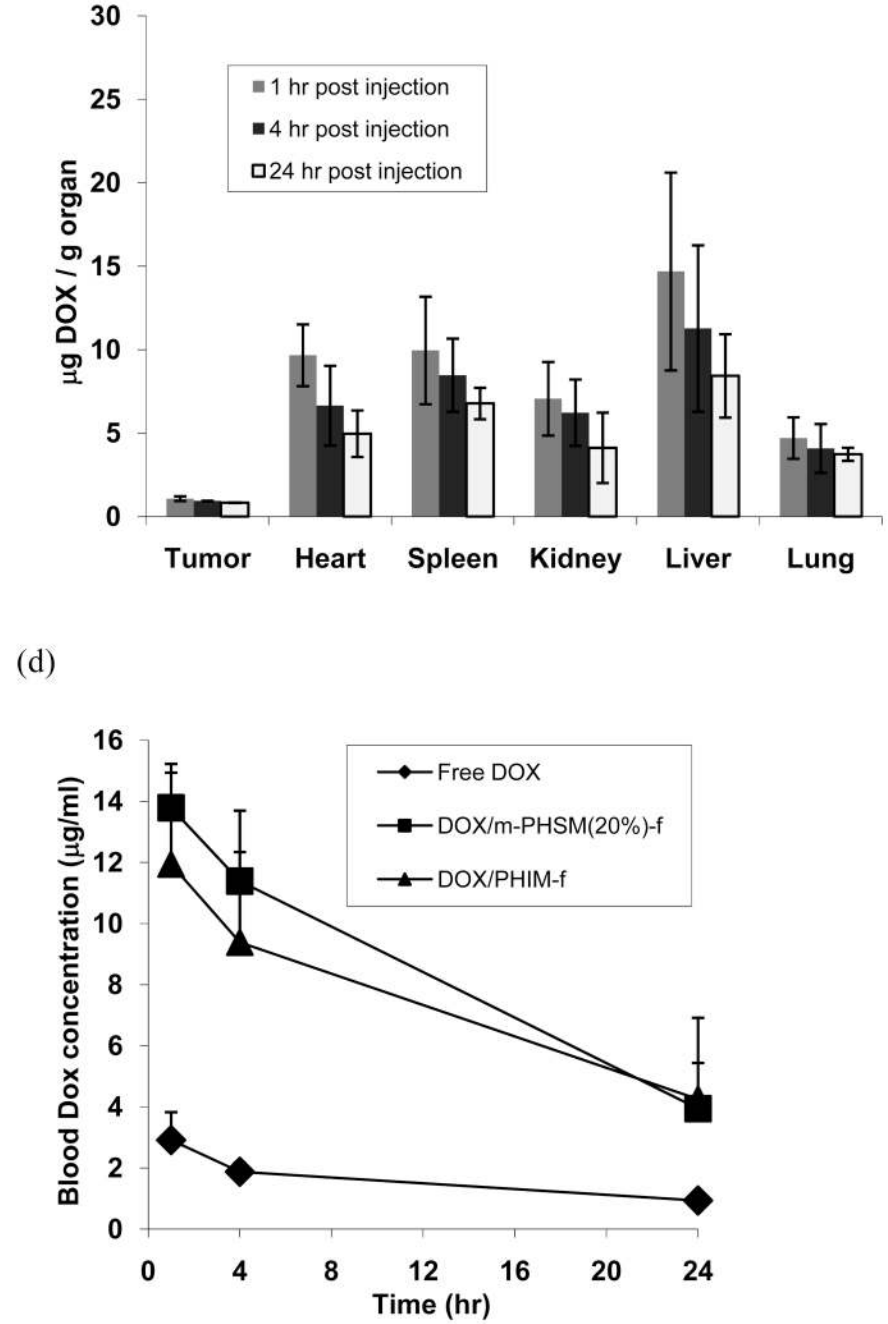

Figure 5.

DOX levels in tissues after IV administration (10 mg/kg DOX equivalent dose) of (a) pH-sensitive micelles (DOX/m-PHSM(20%)-f), (b) pH-insensitive micelles (DOX/PHIM-f), and (c) free DOX in PBS against s.c. human ovarian A2780/DOX^R tumor xenografts. DOX levels in blood (d) of 3 formulations (free DOX, DOX-loaded pH-insensitive micelles (DOX/PHIM-f), and DOX-loaded pH-sensitive micelles(DOX/m-PHSM(20%)-f). Animals were sacrificed at 1, 4, and 24 hr post-injection (n = 4). Values are the mean ± the standard deviations (S.D.).

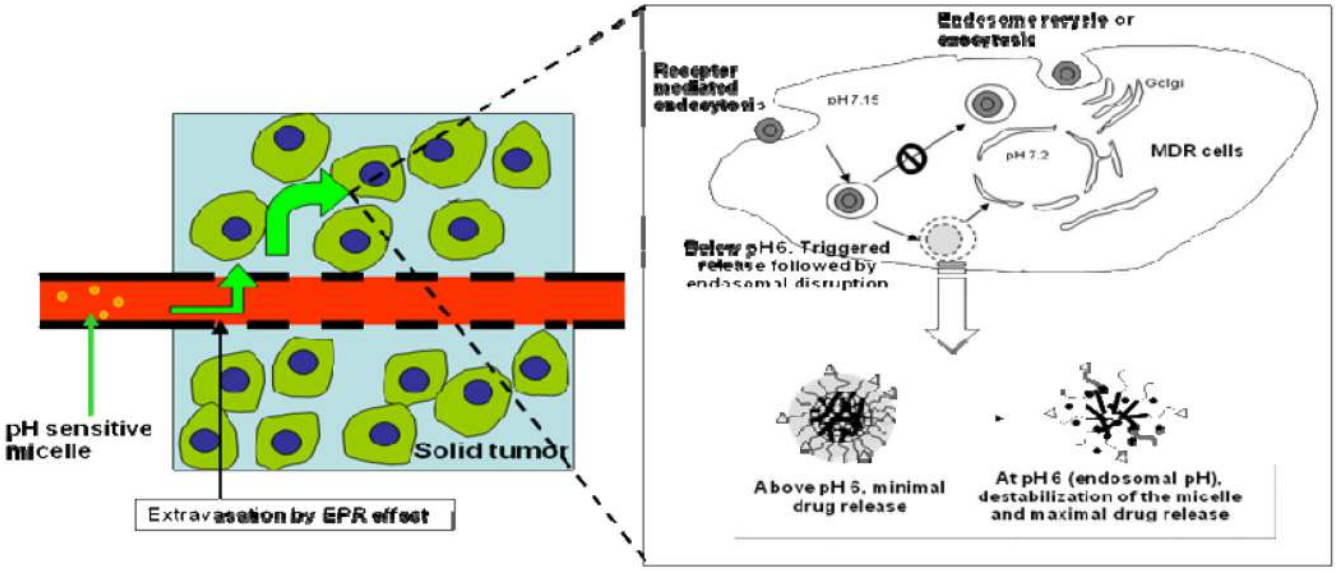

Figure 6.
Schematic picture of the mechanism of pH-sensitive micelle targeting endosomal pH after IV injection.